TIME ACCURATE COMPUTATION OF UNSTEADY SHOCK TUNNEL FLOW WITH COUPLED DIAPHRAGM RUPTURE MECHANICS

D. Scott McRae
M. A. Zikry

Department of Mechanical and Aerospace Engineering
North Carolina State University
Raleigh, North Carolina 27695-7910

29 October 1999

Final Technical Report for the Period 1 August 1995 - 31 July 1999
AFOSR Grant F49620-95-I-0374

Distribution Unlimited

Prepared for

Air Force Office of Scientific Research
AFOSR/MN
801 N. Randolph Street, Room 732
Arlington, VA 22203

REPORT DOCUMENTATION PAGE

AFRL-SR-BL-TR-00-

0200

1. AGENCY USE ONLY (Leave blank)	2. REPORT DATE	3. REPORT TYPE AND DATES COVERED
	29 OCTOBER 1999	FINAL TECHNICAL REPORT- 1 AUGUST 1995 TO 31 JULY 1999

4. TITLE AND SUBTITLE
Time Accurate Computation of Unsteady Shock Tunnel Flow with Coupled Diaphragm Rupture Mechanics

5. FUNDING NUMBERS
AFOSR Grant F49620-95-I-0374

6. AUTHOR(S)

D. S. McRae
M. A. Zikry

7. PERFORMING ORGANIZATION NAME(S) AND ADDRESS(ES)

N.C. State University
Department of Mechanical and
Aerospace Engineering.
Box 7910
Raleigh, NC 27695-7910

8. PERFORMING ORGANIZATION REPORT NUMBER

9. SPONSORING / MONITORING AGENCY NAME(S) AND ADDRESS(ES)

Dr. Len Sakell
AFOSR/MN
Air Force Office of Scientific Research
801 N. Randolph Street, Room 732
Arlington, VA 22203

10. SPONSORING / MONITORING AGENCY REPORT NUMBER

11. SUPPLEMENTARY NOTES

12a. DISTRIBUTION / AVAILABILITY STATEMENT
Unlimited

12b. DISTRIBUTION CODE

13. ABSTRACT *(Maximum 200 Words)*

This report reviews work performed toward the goal of simulating time accurately the initiation of flow in a hypersonic shock tunnel, including coupled diaphragm rupture mechanics. A solution-adaptive mesh Naver-Stokes code was modified to improve mesh distribution for rapidly moving flow features, to include boundary surface motion, and to incorporate weight function and stability enhancements. A simulation of an unadapted grid blade-type shock tube diaphragm opening actuated by algorithm was completed. A repeat of these simulations with mesh adaptation revealed problems with the adaptive algorithm related to the interaction with the grid block structure that were only partially alleviated by limiting mesh movement at the blade tip.

Plane strain and axisymmetric finite-element programs have been developed for the investigation of dynamic inelastic deformation and rupture of a shock-tube diaphragm. Results indicate that crack nucleation occurs when compressive waves at high pressures reflect off the rear of the diaphragm as tensile waves that are a precursor to crack initiation. Results from this study, indicate that stress fields, stress gradients, and plastic strains at the free-edge or at the crack or notch are physically large enough, at the higher pressures, to result in crack nucleation, diaphragm rupture, and material separation

14. SUBJECT TERMS
CFD, shock tunnel, solid mechanics, inelastic strain, crack propagation, stress waves

15. NUMBER OF PAGES
30

16. PRICE CODE

17. SECURITY CLASSIFICATION OF REPORT	18. SECURITY CLASSIFICATION OF THIS PAGE	19. SECURITY CLASSIFICATION OF ABSTRACT	20. LIMITATION OF ABSTRACT
Unclassified	Unclassified	Unclassified	None

Executive Summary

Technical Review

This report reviews work performed toward the goal of simulating time accurately the initiation of flow in a hypersonic shock tunnel, including coupled diaphragm rupture mechanics. Two codes are under development to investigate coupled flow and diaphragm simulation. The fluids code was based on an existing solution-adaptive mesh Naver-Stokes code that had been applied to compute the unsteady flow over stalled compressor blades arranged in a cascade. Initial testing of this code revealed that the mesh movement algorithm, which had performed well when applied to compressor cascades and to a self excited oscillatory flow, was inadequate for the large, high- velocity feature movement present in shock tube- type flows. Modifications were made to effect improved mesh distribution for rapidly moving flow features, to include boundary surface motion in both solver and adapter, and to incorporate weight function and stability enhancements from the NCSU adaptive mesh code SIERRA (Laflin). The mesh movement and block boundary modifications were verified by solving the Riemann problem for conditions with shock speeds similar to those to be encountered in an actual shock tunnel. The boundary movement changes were verified by a piston movement computation, whereas both of these computations served to verify the weight function and stability enhancements. Next a simulation of a shock tube diaphragm opening without grid adaptation was completed. A blade- type diaphragm was chosen to minimize the difficulties associated with hanging blocks during adaptation. When the diaphragm was actuated by algorithm, these simulations revealed two different flow initiation mechanisms, depending on the ratio of surface movement to fluid velocity. Next these simulations were repeated with mesh adaptation. Problems were encountered related to the interaction of the grid block structure with the adaptive algorithm. Limiting mesh movement in the vicinity of the blade tip only partially alleviated these problems. Analysis showed that one of (or a combination of) two further developments would be necessary to complete the fluids code development. The first was to allow non-continuous grids across block boundaries. This was needed to allow

each block to undergo independent grid deformation without imposing the same deformation on neighboring blocks. The second requirement was dictated by the grid deformation upon full opening of the diaphragm. An adaptive unstructured grid code would permit this physical deformation while maintaining grid viability. Both developments are being carried forward under other research projects. and will be available for further exploration of this problem.

During the solid mechanics research, plane strain and axisymmetric finite-element programs have been developed for the investigation of dynamic inelastic deformation and rupture of a shock-tube diaphragm. Modifications have also been applied for the characterization of damage progression and failure evolution pertaining to diaphragm rupture. The dynamic constitutive formulations that were developed account for high pressures, strain-rate, and thermal effects. Specialized numerical techniques have been developed that allow tracking of propagating stress waves in structural components. This is significant, because our results indicate that crack nucleation occurs when compressive waves at high pressures reflect off the rear of the diaphragm as tensile waves that are a precursor to crack initiation. This two dimensional wave reflection was used as a ductile failure criterion to signify crack initiation for high pressure loading conditions. Using this failure criterion, stresses that correspond to the fracture strength of the material have been predicted. The generalized inelastic rate-dependent phenomenological plasticity formulation that accounts for noncoaxial effects such as thermal softening and kinematic and isotropic hardening has been used, with the newly developed failure criteria, to investigate damage progression and failure evolution in rupturing diaphragms. Unnotched, notched, and cracked geometries have been used to analyze the inelastic strain fields that could be associated with either the gradual opening (petal opening), or the instantaneous rupturing of the diaphragm. New methods have developed to track the failure due to the reflected waves. Results from this study indicate that stress fields, stress gradients, and plastic strains at the free-edge or at the crack or notch are physically large enough, at the higher pressures, to result in crack nucleation, diaphragm rupture, and material separation. This buildup in the opening mode stress is directly related to the reflected tensile waves. Based on the

newly developed solid mechanics code for structural integrity, the onset of failure was predicted and used to model petal opening.

Graduate Student Retention

Research progress in this project was limited during the final two years by the very issue that the AASERT program was intended to improve; the reduced number of U.S. citizens entering graduate school in the core engineering disciplines. Of the two students funded initially by this grant, the first, after completing the MS degree and achieving solid progress toward developing a fluids code for this research, chose to accept a lucrative software related position with E-Systems rather than continue for the PhD. The second student who performed the solid mechanics research, after completing an MS, chose to explore other research projects even though continuing for the PhD. In normal times, two U.S. students would have been recruited from our CFD and solid mechanics sequences and the work would have continued with some slowdown for training and code familiarization. However no students from these groups were immediately available. For the fluids research, a student was found, in the process of returning to school after a break in a computational astrophysics MS program, who was interested in a dual AE/Physics degree (BSAE from UVA). However, considerable training in CFD was needed and the student subsequently took a full time software related job off campus because of financial obligations that the RA stipend would not support. Although some work on the fluids code continued beyond this point, little true progress was made toward the final goal. In the case of the solid mechanics student, he returned to the project after a one year hiatus and continued work on the crack propagation and deformation study reported herein. However, no coupling between the two codes was accomplished.

Student Retention Recommendation

Allowance for greatly increased graduate student stipends should be included in future AFOSR/AASSERT grants. The initial reduction in undergraduate student population in the 1990's was clearly, for Aerospace Engineering, due to the negative perceptions of job availability upon graduation. However, now that the undergraduate

AE enrollment is rebounding, the increased availability of lucrative positions at both the BS and MS levels has kept AE graduate enrollment depressed. It is unrealistic to expect many qualified students to forego $30K to $50K in salary differential yearly to enter or remain in graduate school.

Project Personnel

D. Scott McRae, PI

M. A. Zikry, Co-PI

Funded Graduate Research Assistants

Jared Baucom, Ph.D. student (Degree expected 12/2000)

Darren White, completed M.S. degree, August 1997.

G. Christopher Jenkins, M.S. student replacing D. White, August 1997(Degree expected 6/2000)

Publications

M. A. Zikry and J. Baucom (1997), High Pressure Shear Strain Localization in Structural Steel, in Applications of Engineering Plasticity, pp. 371-376, ed: A. Khan, Elsevier Press. A presentation was also given at the Sixth International Plasticity Conference held in Juneau, Alaska, July, 1997.

J. N. Baucom and M. A. Zikry (1999) "Perturbation analysis of high strain-rate shear localization in B.C.C. crystalline materials" Acta Mechanica 137, 109-129.

Thesis

White, D. A., "Computation and Analysis of Hypersonic Shock Tubes Including Diaphragm Rupture Effects," M. S. Thesis, N. C. State University, August 1997.

FLUID MECHANICS SIMULATION

This section will review work performed toward modification and development of the multiblock 2-D Navier-Stokes that was continued from a prior research project. The primary tasks have included improvement of the adaptive algorithm to resolve very rapidly moving solution features, installation of moving surface boundary conditions in both the solver and the adapter, incorporation of stability and accuracy enhancements developed by Laflin (SIERRA), and an initial simulation of an actual shock tube diaphragm opening with flow initiation. The description of these tasks was taken primarily from White. Each will be discussed individually and results will be included where appropriate.

Rapidly Moving Features (Grid Convergence)

The mass weighted algorithm of Eiseman is used in a center of mass approach in the NCSU adaptive algorithm. Expansion of the mass weighted algorithm in a Taylor series yields an elliptic system of partial differential equations. The fundamental mathematical character of an elliptic system must be kept in mind when using this approach for dynamic grid adaption. In previous work by Benson, Ingram, and Neaves, 1 to 5 explicit update steps were been used to solve for the new grid point coordinates. In the majority of these cases the new solution was only a small perturbation of that on the previous grid, thereby requiring that the grid node move only a small distance per time step. This offers the benefit of being much more computationally affordable than actually driving the elliptical PDE system to convergence at each time step. For steady state solutions or solutions with well resolved time histories (i.e., small time steps), this approach has been shown to produce excellent results (Benson, Ingram, Neaves, and Laflin). However, poor results were obtained when the standard number of mass-weighted algorithm passes were used in the shock tube calculations, especially when the shock and expansion waves were highly resolved. When the waves moved into the evacuated area in one time step, the resolution was not sufficient to maintain consistent

solution accuracy. After some analysis, it was discovered that iterating the elliptical problem until convergence was approached resulted in a much more even distribution of mesh nodes in regions of constant weight function.

The elliptic center of mass algorithm does provide the necessary propagation of information throughout the domain provided that the solution is allowed to converge sufficiently. For full mathematical ellipticity, the effect of moving one grid point in the domain must influence the position of every other grid point within the domain. Obviously a few explicit point-Jacoby iteration steps cannot provide the necessary global propagation of solution information.

The needed convergence of the grid equations can be achieved through an explicit point Jacoby algorithm only if a sufficient number of iterations are performed. For increased efficiency, a successive over-relaxation (SOR) scheme was implemented. For highly dynamic cases requiring many iterations to relax the mesh, an implicit alternating direction line SOR scheme was used to further speed up the numerical propagation of information throughout the domain. Generally speaking, the purpose of the explicit SOR and implicit algorithms was to increase the numerical domain of dependence of the solution, not to provide increased local point movement. If the flow features being tracked are moving rapidly enough, an explicit SOR or an implicit adaption algorithm can result in locally high grid velocities. Special care must therefore be taken with these schemes to limit the range of point movement to ensure that grid lines do not cross. In order to prevent crossover, a grid point must not be allowed to move outside its dual cell at each iteration of the grid solver. A numerical experiment demonstrating the significance of grid convergence is presented in the Results Section.

Since one of the goals of this research was to couple the diaphragm opening with the fluid dynamics using a solution adaptive mesh, means were developed to adjust for boundary movement while adapting the mesh internally. The general integral governing equation for fluids can be written

$$\frac{\partial}{\partial t}\int_v U dV - \oint_s U\vec{\dot{x}}\cdot d\vec{s} + \oint_s \vec{A}\cdot d\vec{s} = 0$$

where $\dot{\vec{x}}$ is a general vector denoting the movement of a specific cell side relative to the inertial mesh. In the original adaptive algorithm, this vector was non-zero only in

response to changes in the solution. However, when the outer boundary of the mesh must be moved, as in this case, additional movement must be superimposed on the mesh to prevent crossover and/or "piling up" of mesh points adjacent to the moving surface. The vector $\dot{\bar{x}}$ was then separated into two vectors

$$\dot{\bar{x}}=\dot{\bar{x}}_a+\dot{\bar{x}}_b$$

such that $\dot{\bar{x}}_a$ was grid motion due to the adaption and $\dot{\bar{x}}_b$ was grid motion required by boundary movement. The vector $\dot{\bar{x}}_b$ remains in the flow solver portion of the split algorithm, since the flow must respond to boundary movement in the inertial frame. This cell side velocity was determined by approximating a Laplacian distribution over the domain. The vector $\dot{\bar{x}}_a$ was determined in the adaption step and was used in the solution update step as before. In order to ensure that grid crossover does not occur, movement was restricted to a dual cell in the standard adaptive stencil.

Boundary conditions for both fixed and moving solid walls require that ghost cell values of the primitive variables be set such that there is no mass flux through a solid wall. For inviscid walls, the slip condition requires that the ghost cell velocity tangent to the wall be equal to the tangential velocity of the first interior cell. The normal component of the velocity in the ghost cell must be defined such that the interpolated normal component of the fluid velocity at the wall is equal to the normal component of the wall speed. For an η=constant surface, this condition yields the following first order relations for the ghost cell values of velocity:

$$u_{s+\frac{1}{2}}=2\left[\frac{\dot{x}\eta_x^2+(\dot{y}-v_{s-\frac{1}{2}})\eta_x\eta_y+u_{s-\frac{1}{2}}\eta_y^2}{(\eta_x^2+\eta_y^2)}\right]-u_{s-\frac{1}{2}}$$

$$v_{s+\frac{1}{2}}=2\frac{\eta_y}{\eta_x}\left\{\left[\frac{\dot{x}\eta_x^2+(\dot{y}-v_{s-\frac{1}{2}}\eta_x\eta_y+u_{s-\frac{1}{2}}\eta_y^2}{(\eta_x^2+\eta_y^2)}\right]-u_{s-\frac{1}{2}}\right\}+v_{s-\frac{1}{2}}.$$

Here, the subscript (s) refers to the wall, $(s+1/2)$ refers to the ghost cell value, and $(s-1/2)$ refers to the value in the first interior cell. Similar relations are derived for ξ=constant boundaries.

For a viscous wall, the no slip condition must be satisfied. The ghost cell values of velocity must be set such that the fluid and wall velocity are exactly equal. These conditions yield the first order relationships:

$$u_{s+\frac{1}{2}} = 2x - u_{s-\frac{1}{2}}$$

and

$$v_{s+\frac{1}{2}} = 2y - v_{s-\frac{1}{2}}$$

for viscous walls.

Solid walls were assumed to be adiabatic and the normal component of the momentum equation was used to obtain pressure. The remaining conditions for inflow, outflow, and grid block boundaries were identical to those implemented by Ingram.

A final change was necessary to accommodate moving boundaries. The parametric space adaption was continued although a modification was required. After a solver time step was completed, the physical boundary has now been allowed (potentially) to move to a new location. If the boundary point moves into the interior of the original domain, then a transformation exists to remap the point back into the physical space after the adaption procedure. However, if the point moves outside the domain, no transformation exists to allow the correct remapping. A solution to this problem was to reset the parametric space back to its originai state (i.e., having integer coordinates) and then define a new transformation at the beginning of every call to the adapter. The adapter then iterates the grid to the appropriate level of convergence in the new parametric space and correctly maps the solution back to the physical space, preserving the time accuracy of the prescribed boundary motion.

The weight function used in the center of mass algorithm serves to control the amount and location of point clustering. More recent work by Laflin and McRae also stresses the improvements obtained by aligning the grid with the flow features. Laflin

derives a weight function based on a solution interpolation error approximation (SIERRA) which serves to both refine and align the grid to the solution.

During the course of this work, a variety of weight function formulations were examined. In evaluating the weight functions, it is important to first appreciate the effects of the rapid movement of the feature. In a temporally evolving solution, if the grid is heavily refined over only a cell or two, then the flow feature may potentially move into a less refined region during the next time step thereby mitigating the benefits of the adaption process. Ideally, the grid must be sufficiently refined over the entire region traversed by the flow feature through a time step. Since the grid adapter does not have access to future solution data, the grid cannot be adapted to provide the exact refinement required over the forthcoming time step. Considering that the weight function is in essence a measure of the desired mesh density, an arbitrary weight function should contain local extrema in the regions requiring the most grid point movement. Localized smoothing of this function would diffuse the extrema, thereby producing a smoother variation in cell volumes and providing an increase in the radius of clustering that is proportional to the amount of smoothing. With sufficient smoothing, the resulting grid will generally be adequately refined over the domain traversed by a flow feature throughout the next time step.

Examination of weight functions based on first and second derivatives of the primitive fluid variables revealed that both provided an excellent locator of regions requiring adaption at a minimum of computational effort. First derivative weight functions, however, do possess the drawback of overadapting the interior of expansion waves. Second derivative, or curvature based weight functions help to alleviate this problem.

Experimentation with Laflin's SIERRA weight function has shown to provide results almost identical to those obtained by more cost effective curvature methods in one dimensional problems. For two dimensional problems, the SIERRA weight function tends to result in less grid shear for certain problems. For the nearly 1-D solutions presented herein, the increases in performance do not seem to offset the extra computational expense however. For this reason, the weight function used for this work was based on second derivatives evaluated in the computational space and seemed to

provide a balance between cost and performance. SIERRA will be used for more complex flows. Separate weight functions were computed for each coordinate direction to allow greater control over the adaption process.

Square Wave Validation of Grid Convergence Requirement

A simple numerical experiment was used to demonstrate the effects of grid convergence. An analytically defined square wave was allowed to propagate through a long narrow channel, similar to the movement of a shock wave in a shock tube, and the ability of the adaption algorithm to track the wave was observed. The square wave had a peak value of 100, a minimum value of 1, and traveled in the positive x-direction with velocity 1 on an initial grid of 201 □ 21 points. Figure 1 shows the movement of this wave through the domain and the adapted grids at four instances in time. In this case, the adaption algorithm makes 20 explicit iterations per time step. The discontinuities was resolved well initially and the remainder of the domain was left with a generous number of points. As the discontinuities continue traveled down the channel, increasingly more grid points were drawn from upstream to resolve the advancing wave fronts and then remained where unneeded in the downstream region. This process can lead to the near total evacuation of points from the region upstream of the discontinuities. If a Navier-Stokes solver were coupled with a grid that behaved in this manner, the increasing cell size in the region of the discontinuities could lead to an unstable solution. Note that this phenomenum is not a problem (and in fact may be desirable) for steady or slowly varying solutions.

The observed grid results from the fact that the grid equations were not converged to a solution that was truly elliptic in nature. The solution to this problem was to bring the grid closer to convergence each time the adaptor was applied. Unfortunately, increasing grid convergence increased the cost of obtaining the solution.

Figure 2 presents the same square wave, but this time the adaption algorithm used 200 implicit iterations per time step. In this case, the grid remains finely adapted in the discontinuous regions and evenly distributed throughout the remainder of the domain. By allowing the grid to advance to a sufficiently converged solution, any local

changes in the grid were felt by distant grid points and the entire grid was adjusted to accommodate the local refinement.

Diaphragm Rupture Without Adaption

After installation of moving boundary capability and other code improvements, the first step leading to coupling with the solid mechanics code was to couple with controlled diaphragm motion. The diaphragm shape and motion are not realistic but were chosen to allow assessment of expected problems with grid behavior upon rupture.

A four block grid, each block having 75x50 grid points, was used to model the domain. The shock tube had length 10, a radius of .5, and the diaphragm was assumed to have ruptured initially without motion and to have an initial opening radius of .05. The diaphragm was .05 units thick at the tunnel wall and tapered down to a sharp point near the centerline. The diaphragm was initially symmetric and centered about the line x=0. Two grid blocks abut the diaphragm and the remaining two blocks span the distance between the centerline and the tip of the diaphragm. The deformation of the diaphragm was governed by a linear decrease in $\dot{y}_b$ from the tip velocity to zero at the wall and a cubic decrease in $\dot{x}_b$ from the tip velocity to zero at the wall. Initial conditions for this case were similar to those of a standard shock tube problem. The pressure ratio across the diaphragm was 10:1, the density ratio was 8:1, and the flow was initially at rest.

Figure 3 shows the time history of the opening process from t=0 to t=0.99 for the case of a diaphragm tip velocity of 0.1 and no grid adaption. The typical features associated with a 1-D shock tube were observed, but here the waves were curved because the streamlines converge while approaching the diaphragm and diverge after passing through the diaphragm. Following a streamline, fluid from the driver section of the tube accelerates to supersonic velocities through the small opening in the diaphragm before being slowed to subsonic velocities by a shock further downstream. The contact discontinuity formed at flow initiation then occurs. The jet of fluid is separated from the quiescent flow into which it is entering by a bow shock. As the jet enters the driven section, it entrains fluid from behind the diaphragm resulting in the

formation of a vortex behind the tip. This vortex is then convected downstream into the driven section. The last frame in Figure 3 shows that the jet has expanded to reach the outer wall of the tube and the bow shock is now nearly planar. The flow along the wall of the tube develops a boundary layer which the unadapted grid does not resolve.

Figure 4 shows the time history of the opening process from t=0 to t=0.33 for the case of a diaphragm tip velocity of 0.3 and no grid adaption. At the end of this run, the diaphragm deformation was equal to that at the end of the run in Figure 3. The same features observed for the case with tip velocity of 0.1 develop for this case with the exception of the vortex roll-up behind the tip. Because the induced fluid velocity behind the diaphragm nearly matches the jet velocity, the formation of the tip vortex is inhibited. Additionally, the run was stopped to ensure a diaphragm displacement equivalent to that of the previous case, therefore the jet has not yet expanded to the diameter of the tube.

Diaphragm Rupture With Adaption

The adaptive algorithm, as originally formulated for fixed boundary problems, does not yet provide useful adaption in the vicinity of the simulated diaphragm tip. The grid block topology in this region leads to a concave grid boundary, even in parametric space. This leads to severe problems with grid line crossover near the time an exponentially decaying grid movement restriction function centered at the tip results in the interim solution of Figure 5. Analysis of these results indicates that the blocks must be modified to allow discontinuous grid lines across the boundary. This will allow independent adaption in each block and alleviate much of the skewness evident in Figure 5.

It is apparent from these cases that changing the rate at which the diaphragm opens affects the flow structure. It will therefore be critical in future work to accurately determine how the diaphragm deforms in response to the dynamic loads imposed by the fluid. In preparation for coupling with the solid mechanics code, Figure 6 shows an initial mesh as it deforms with the initial deformation of the diaphragm geometry in use for the solids code development. Also, numerical experiments were conducted to examine the flow structure after the shock wave reflects from the tunnel wall. An

example of the complex structure of the resulting shock-wave boundary layer interaction as resolved by the adaptive mesh code is shown in Figure 7. Note the jet of flow near the wall entering the stationary fluid region (similar to that shown in Weber and Oran). The status of the solid mechanics portion of the work follows.

SOLID MECHANICS SIMULATION

During the solid mechanics research, plane strain and axisymmetric finite-element programs have been developed for the investigation of dynamic inelastic deformation and rupture of a shock-tube diaphragm. Modifications have also been applied for the characterization of damage progression and failure evolution pertaining to diaphragm rupture. The dynamic constitutive formulation that were developed account for high pressures, strain-rate, and thermal effects. Specialized numerical techniques have been developed that allow tracking of propagating stress waves in structural components. This is significant, because present results indicate that crack nucleation occurs when compressive waves at high pressures reflect off the rear of the diaphragm as tensile waves that are a precursor to crack initiation. This two dimensional wave reflection was used as a ductile failure criterion to signify crack initiation for high pressure loading conditions. Using this failure criterion, stresses that correspond to the fracture strength of the material have been predicted. The generalized inelastic rate-dependent phenomenological plasticity formulation that accounts for noncoaxial effects such as thermal softening and kinematic and isotropic hardening has been used, with the newly developed failure criteria, to investigate damage progression and failure evolution in rupturing diaphragms. Unnotched, notched, and cracked geometries have been used to analyze the inelastic strain fields that could be associated with either the gradual opening (petal opening), or the instantaneous rupturing of the diaphragm. New methods have developed to track the failure due to the reflected waves. Results from this study indicate that stress fields, stress gradients, and plastic strains at the free-edge or at the crack or notch are physically large enough, at the higher pressures, to result in crack nucleation, diaphragm rupture, and material separation. This buildup in the opening mode stress is directly related to the reflected tensile waves.

Computational Method

The current deformation state is obtained by updating the total deformation tensor, the plastic deformation-rate tensor, and the equation of state as a function of the current pressure and particle velocities. The total deformation rate tensor and the total spin tensor are obtained by an explicit finite-element method. The equations of motion are integrated, by the central difference method, to obtain the nodal accelerations, the nodal velocities and the nodal displacements. The plastic deformation-rate tensor is obtained by the derivation of an initial value system of equations. This is based on a method developed by Zikry (1994). This initial value system of equations is integrated by a combination of explicit multistep and implicit A-stable methods. A family of A-stable methods is used where numerical stiffness of the initial value system may arise due to plastic wave speeds at the interface. The stiffness ratio is used to automatically switch solution methods between the explicit and the A-stable methods. The validity of the present algorithm has been tested by simulating the axisymmetric deformation of several plasticity problems (no noncoaxial effects) for which known numerical solutions exist.

An unnotched, undeformed diaphragm, with a pre-existing central through-crack (Fig. 8A), was subjected to pressures ranging from 0 to 104 psi. The diaphragm was modeled as a cantilevered plate with a free end, to simulate the through-crack. A uniform pressure was applied transversely, along one side. Two rates of pressure application were examined: an instantaneous load application and a ramp load. This was done to determine the effects of loading rate. For the slower rate of loading, the pressure was applied linearly from an undeformed state (Fig. 8B). To gain a more detailed understanding of the deformation modes associated with these meshes, contours of effective plastic strains are given at pressures of 3000 psi, 6000 psi, and 7000 psi (Figs. 9-11). As shown in Fig. 10, at a pressure of 6000 psi (30 ms), the effective plastic strain has attained a maximum value of more than 43% near the fixed edge. As these contours also indicate, large plastic-strain gradients have developed in a small region near the fixed edge. Maximum effective plastic strains range from approximately 0% to 70%, when the diaphragm penetrates the plane of the fixed edge

(at approximately 35 ms). Results for the impact load were qualitatively similar, but the diaphragm had penetrated the plane of the fixed edge at approximately 15 ms(Fig. 11).

The deformed mesh at face pressures of 3000 psi, 6000 psi, and 7000 psi are also shown in Figs. 9-11. A highly refined mesh was used near the fixed end, in the region of high plastic strain gradients, and in the crack-tip region. These refined meshes enabled us to resolve the high stress gradients associated with crack-tip plasticity and high pressures.

Impact

Based on the newly developed solid mechanics code for structural integrity, the onset of failure was predicted and used to model petal opening. The solid mechanics code should be coupled interactively to the fluid mechanics code for fully three-dimensional simulations and modeling of material response.

FUTURE WORK

Fluid Dynamic Code

Further development of the adaptive grid algorithm will be needed to resolve the complex geometry and flow movement associated with diaphragm opening. This will take two primary directions:

1) Development of non-continuous grid block boundaries so that adaption can be independent between blocks. This should alleviate the severe restrictions on adaption at concave physical corners.
2) Development of a hybrid structured/unstructured grid approach to improve ability to couple with geometry during the final stages of the opening and also the 3-D rupture geomeries.
3) Development of coupling protocols with the solid mechanics code.

Solid Mechanics Code

1) Development of coupling protocols with the fluid mechanics code.
2) Extension of the code to 3-D..

PERSONNEL SUPPORTED

Jared Baucom, Ph.D. student(degree expected 12/2000)

Darren White, completed M.S. degree, August 1997.

G. Christopher Jenkins, M.S. student replacing D. White, August 1997(Degree expected 6/2000)

Other Participating Personnel

D. Scott McRae, PI

M. A. Zikry, Co-PI

PUBLICATIONS

M. A. Zikry and J. Baucom (1997), High Pressure Shear Strain Localization in Structural Steel, in Applications of Engineering Plasticity, pp. 371-376, ed: A. Khan, Elsevier Press. A presentation was also given at the Sixth International Plasticity Conference held in Juneau, Alaska, July, 1997.

J. N. Baucom and M. A. Zikry (1999) "Perturbation analysis of high strain-rate shear localization in B.C.C. crystalline materials" Acta Mechanica **137**, 109-129.

Thesis

White, D. A., "Computation and Analysis of Hypersonic Shock Tubes Including Diaphragm Rupture Effects," M. S. Thesis, N. C. State University, August 1997.

REFERENCES

Ingram, C.L., *Extension of a Dynamic Solution-Adaptive Mesh Algorithm and Solver to General Structured Multi-Block 2-D Grid Configurations*, Masters' Thesis, North Carolina State University, May 1995.

Benson, R.A. and McRae, D.S., "A Solution-Adaptive Mesh Algorithm for Dynamic/Static Refinement of Two and Three Dimensional Grids," *Proceedings of the Third International Conference on Numerical Grid Generation in Computational Fluid Dynamics and Related Fields*, Barcelona Spain, June 1991.

Benson, R. A. and McRae, D. S., "Unsteady Transients in a Supersonic Inlet Subject to Freestream Perturbations and Dynamic Attitude Changes", AIAA 94-0581, 32nd Aerospace Sciences Meeting, Reno, NV, Jan. 1994.

Laflin, K.R. and McRae, D.S., "Solution-Dependant Grid-Quality Assessment and Enhancement," *Proceedings of the Fifth International Conference on Numerical Grid Generation in Computational Fluid Dynamics and Related Fields*, Starkville MS, April 1996.

Neaves, M. D. and McRae, D. S., "Numerical Investigation of the Unstart Phenomena in an Axisymmetric Supersonic Inlet," Proceedings, International Symposium on Computational Fluid Dynamics in Aero Propulsion, ASME International Congress and Exposition, San Francisco, CA, Nov. 12-17, 1995, pp. 149-156.

Weber, Y.S., Oran, E.S., Boris, J.P., and Anderson Jr., J.D., "The numerical simulation of shock bifurcation near the end wall of a shock tube," *Phys. Fluids*, vol.7, pp. 2475-2488, 1995.

White, D. A., "Computation and Analysis of Hypersonic Shock Tubes Including Diaphragm Rupture Effects," M. S. Thesis, N. C. State University, August 1997

M. A. Zikry and J. Baucom, (1997) High Pressure Shear Strain Localization in Structural Steel, in Applications of Engineering Plasticity, , pp. 371-376, ed:. Khan, Elsevier Press

M. A. Zikry (1994), "An Accurate and Stable Algorithm for High Strain-Rate Finite Strain Plasticity," *Computers and Structures 50*, 337-350

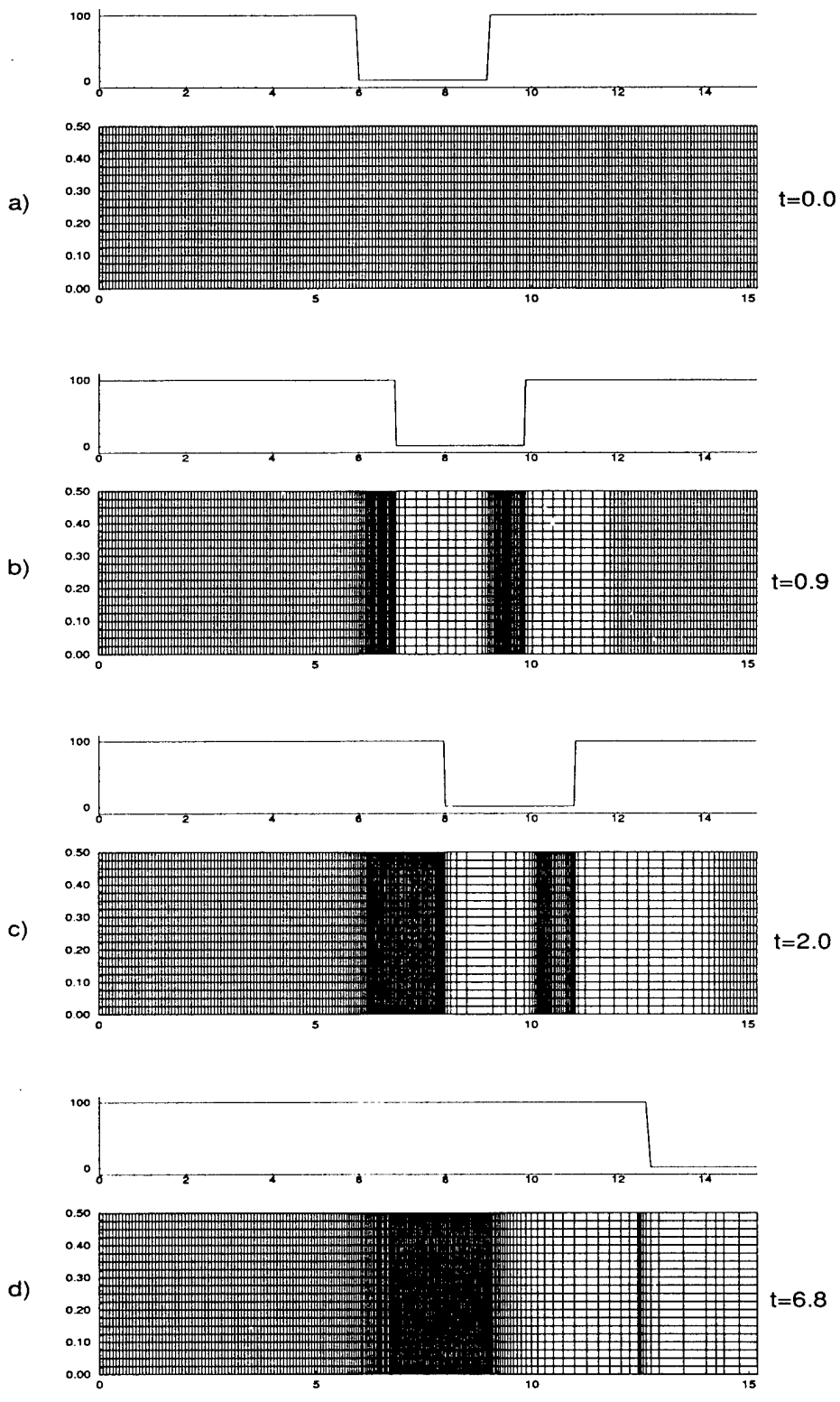

Figure 1: Square Wave With 20 Grid Iterations

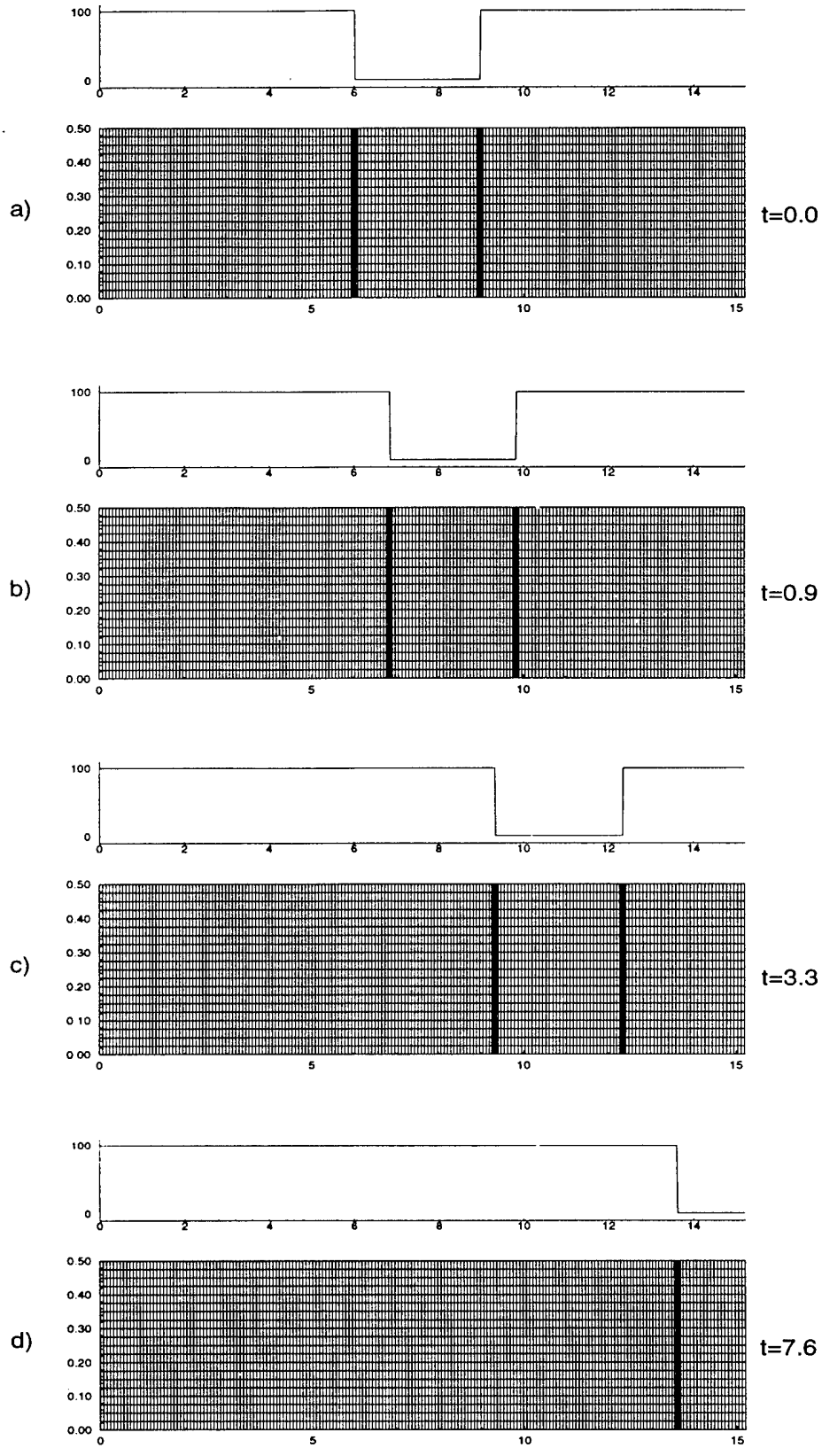

Figure 2:Square Wave With 200 Grid Iterations

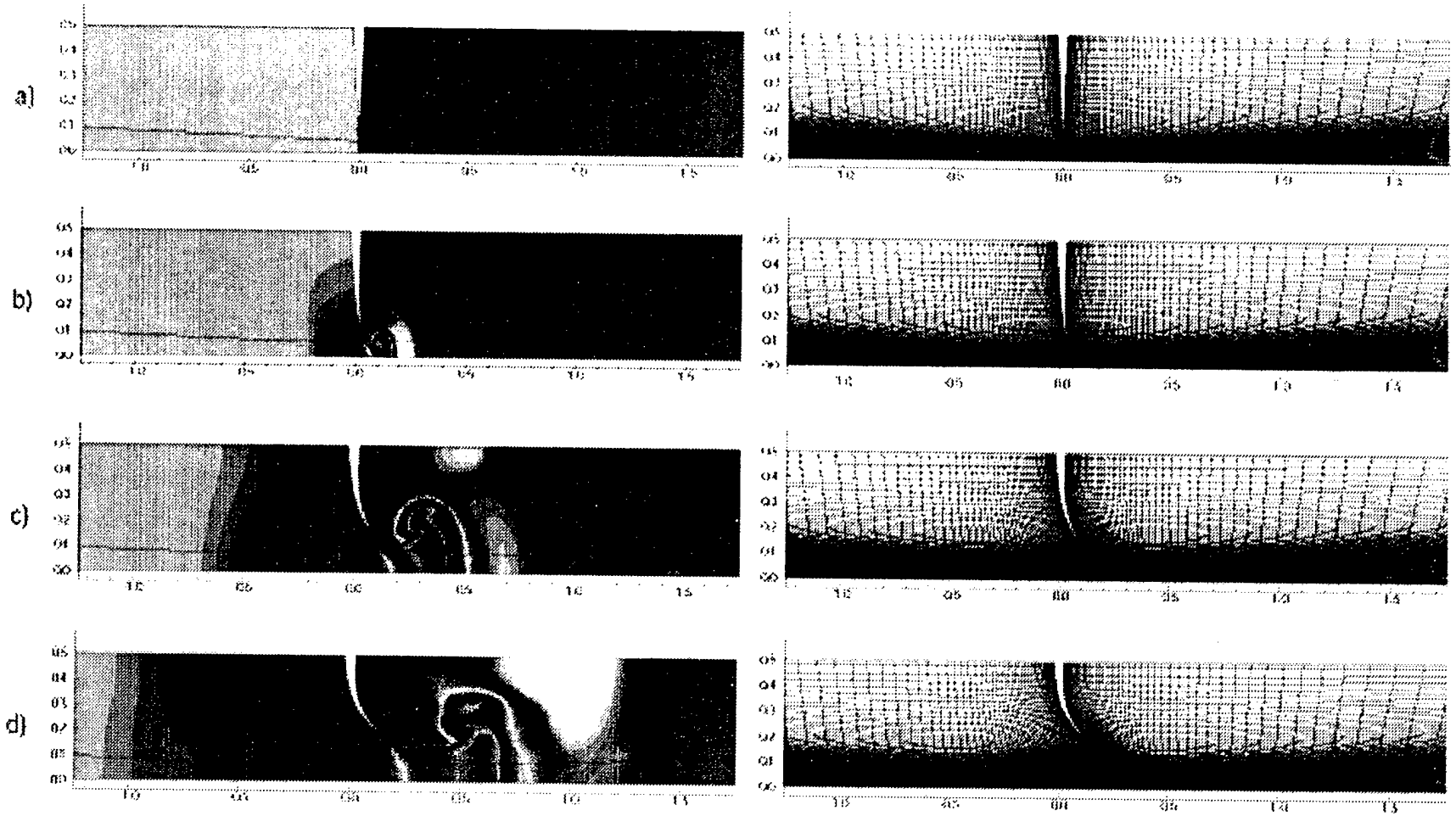

Figure 3: Slow Unadapted Diaphragm Opening

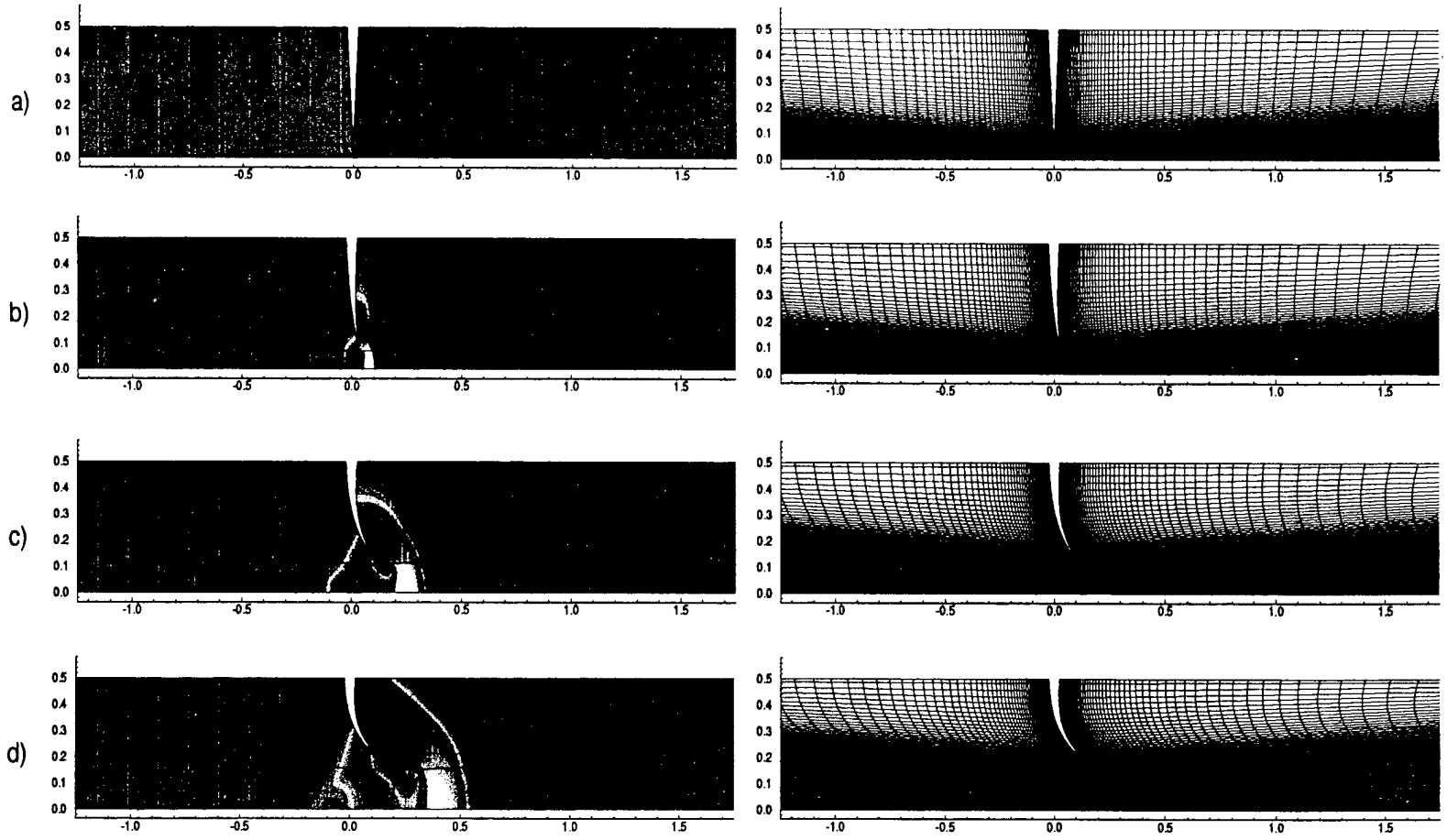

Figure 4: Fast Unadapted Diaphragm Opening

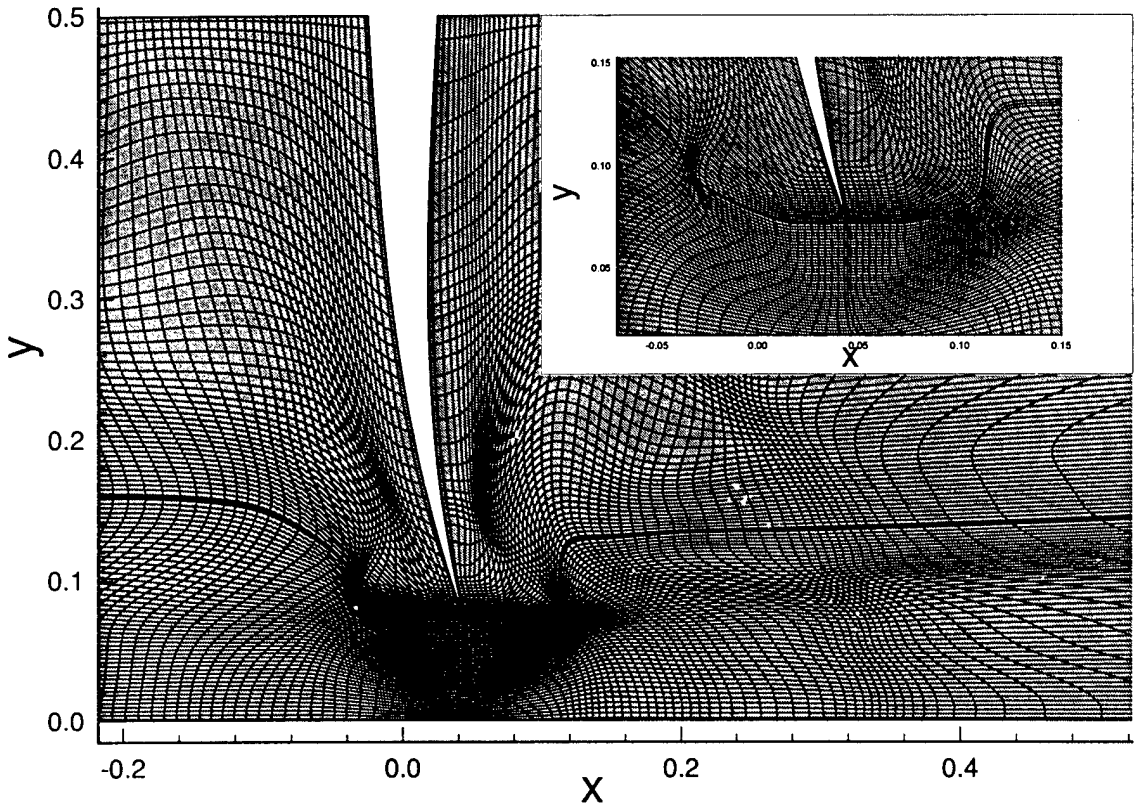

Figure 5: Adapted Mesh Diaphragm With Local Crossover Prevention

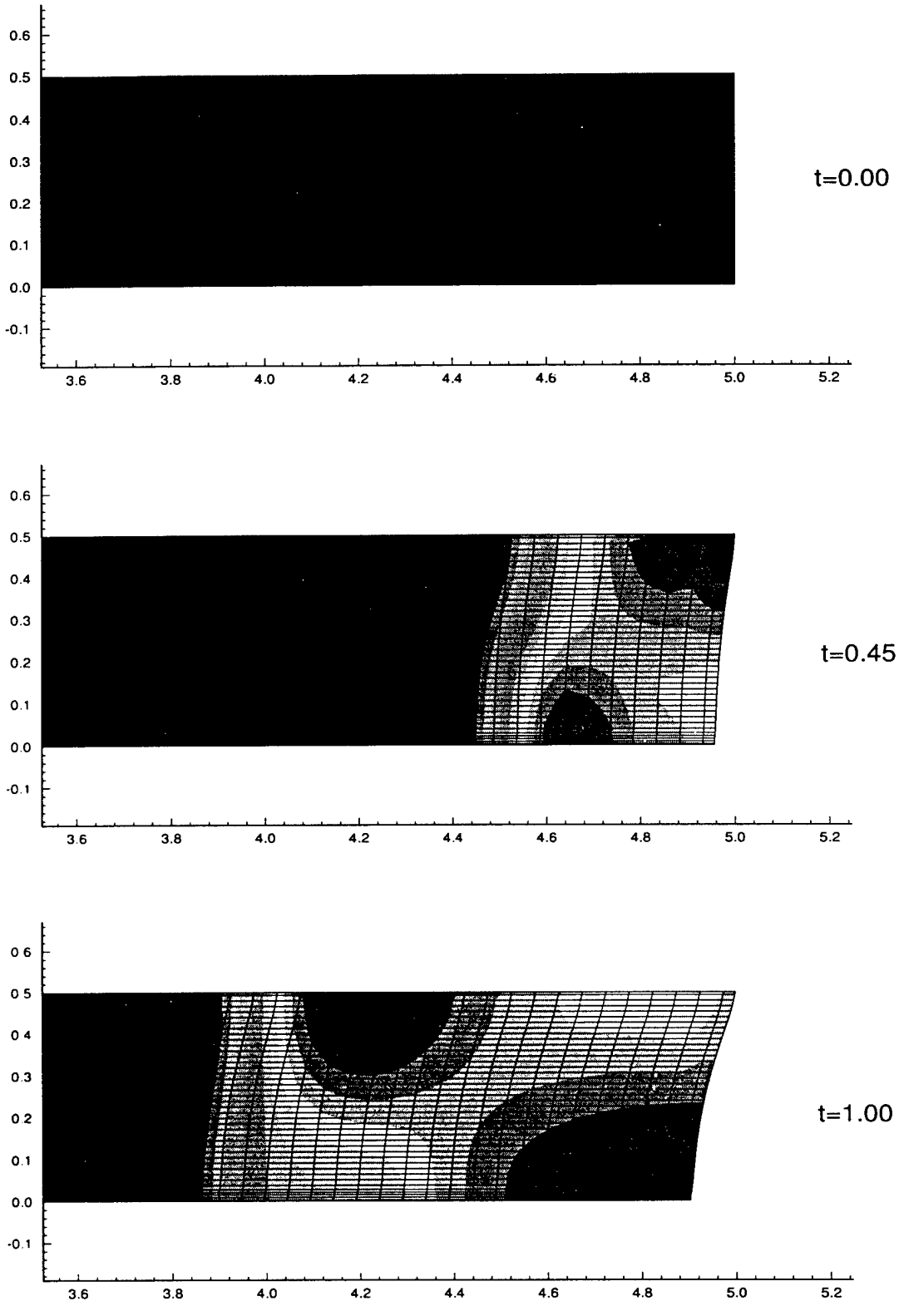

Figure 6: Initial Coupling of Moving Mesh and Solid Mechanics Deformation

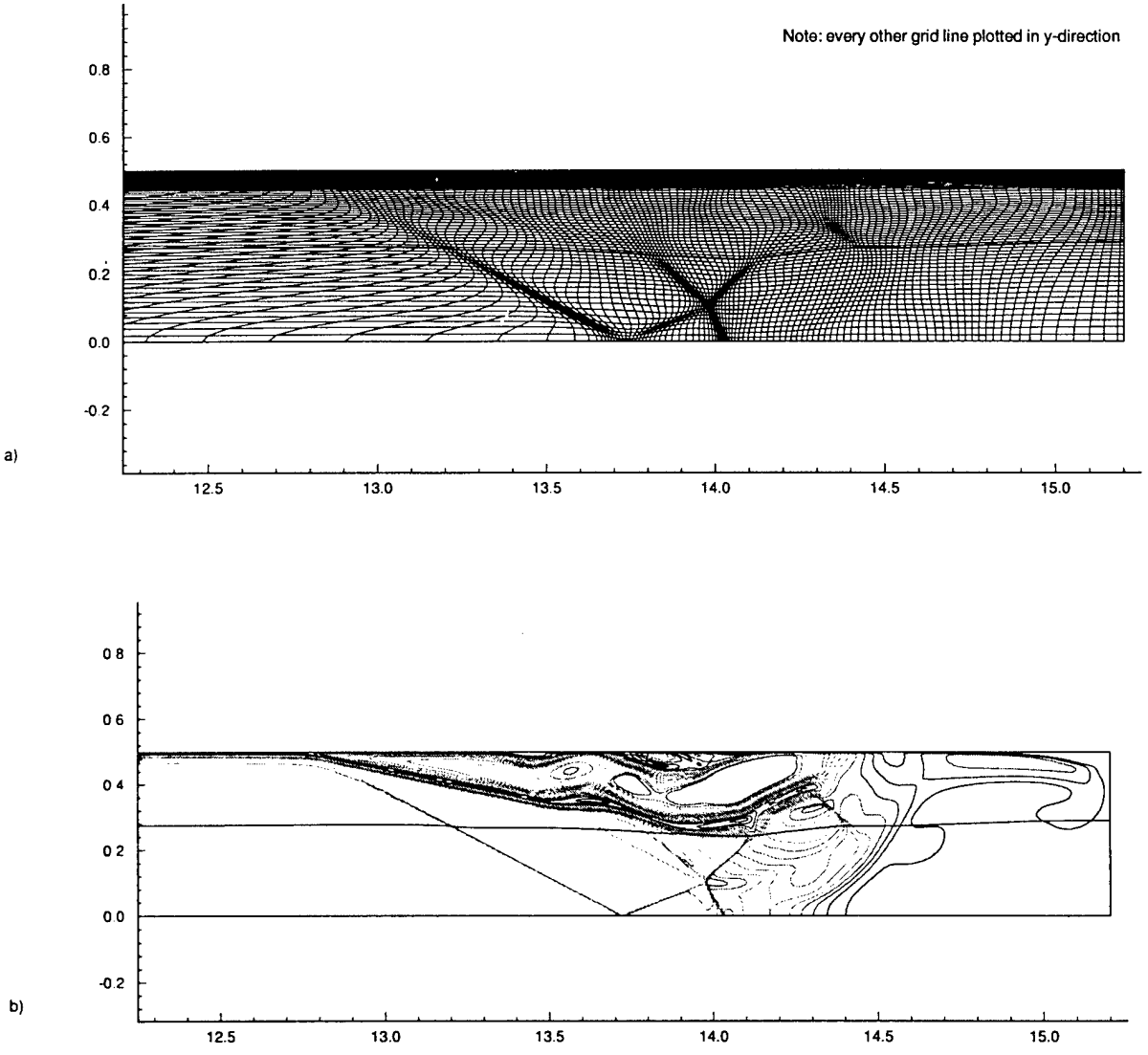

Figure 7: Adapted Shock Wave Reflection from Tube Endwall

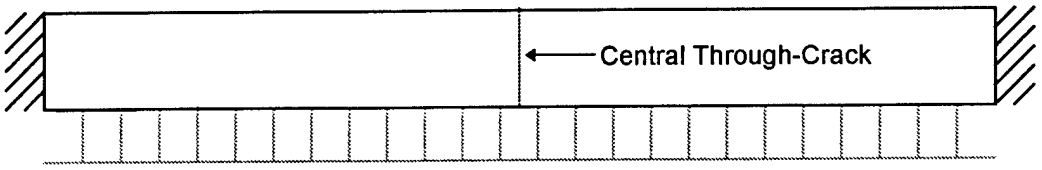

Pressure Load: P

A:

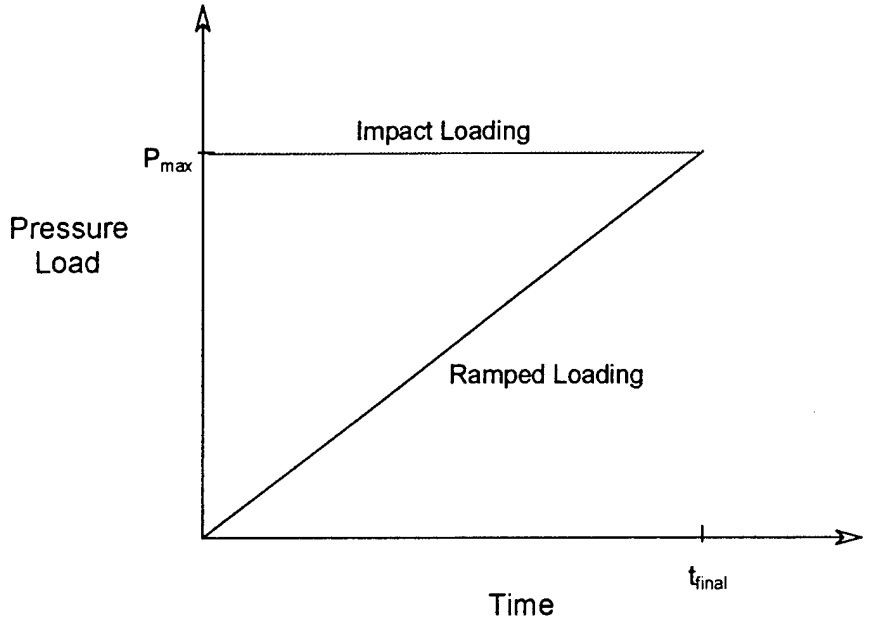

B:

Figure 8A,B: Loading Distribution and Onset

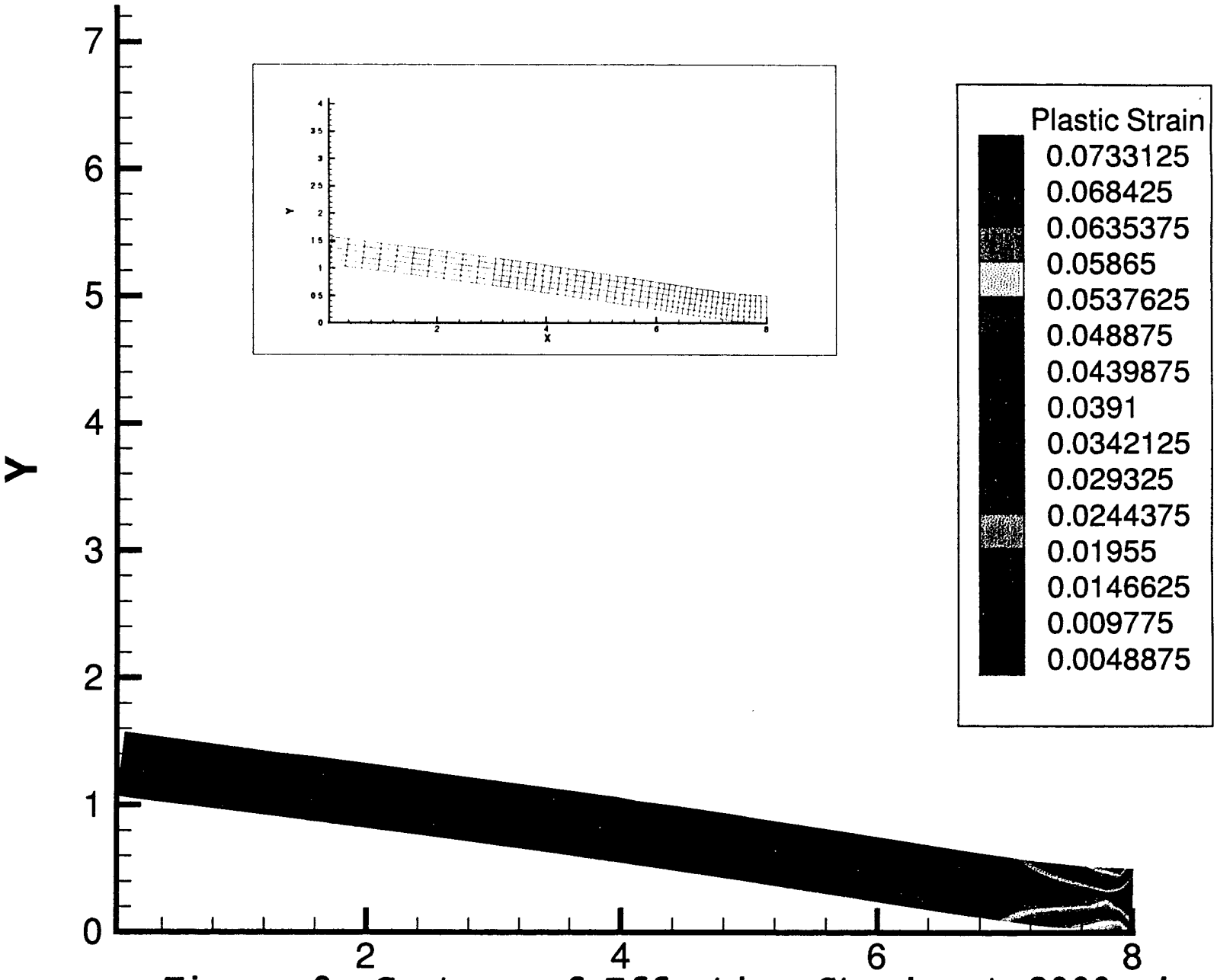

Figure 9: Contour of Effective Strain at 3000psi

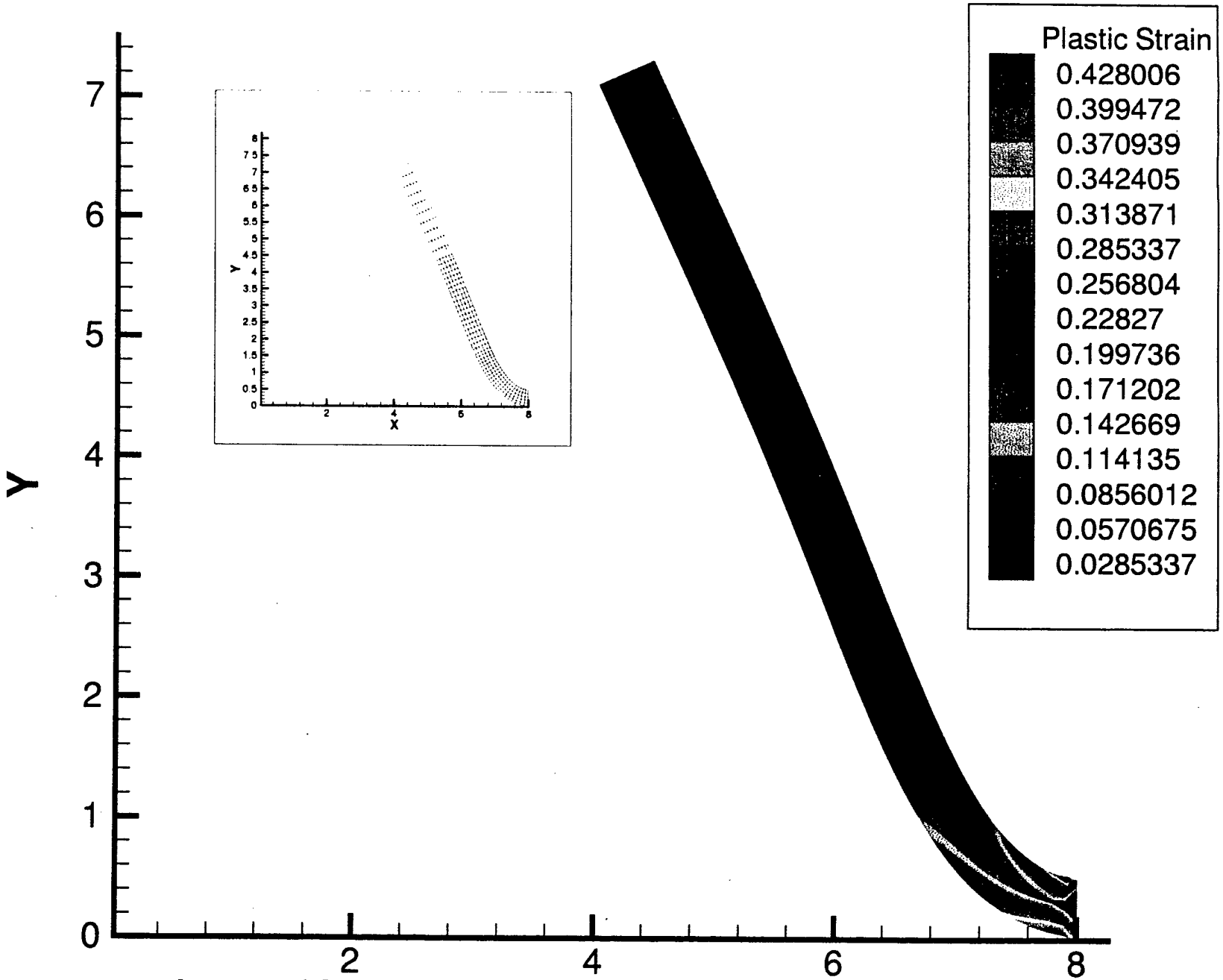

Figure 10: Contour of Effective Strain at 6000psi

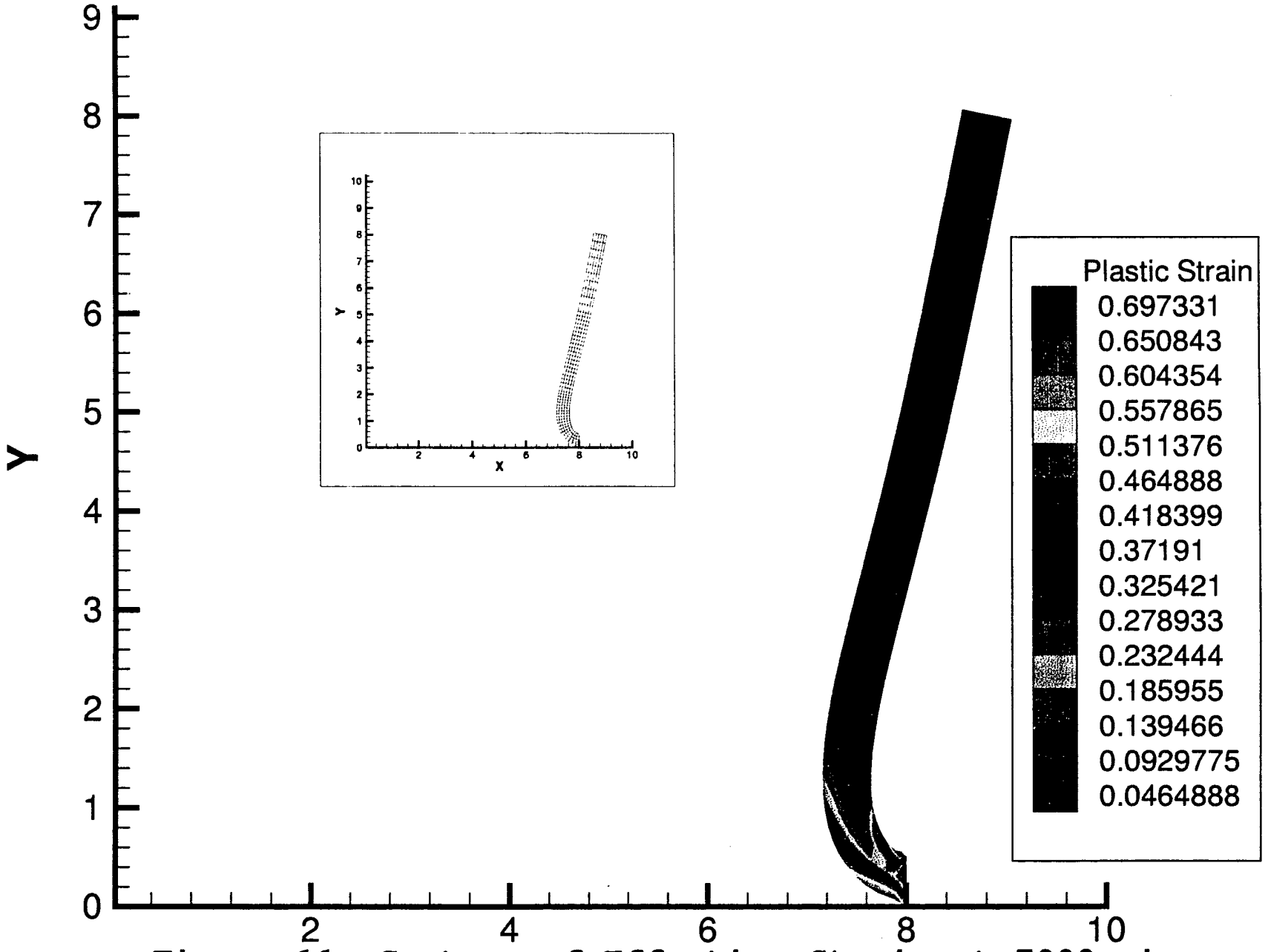

Figure 11: Contour of Effective Strain at 7000psi